IEEE Access
Multidisciplinary | Rapid Review | Open Access Journal

Received December 23, 2019, accepted January 30, 2020, date of publication February 3, 2020, date of current version February 11, 2020.

Digital Object Identifier 10.1109/ACCESS.2020.2971338

On Simple-Sectored Multi-Probe Anechoic Chamber Design for mmWave Adaptive Terminal

XIAOLI YANG[1], WEI FAN[2], NAN MA[1], JIANQIAO CHEN[1], AND PING ZHANG[1], (Fellow, IEEE)

[1]State Key Laboratory of Network and Switching Technology, Beijing University of Posts and Telecommunications, Beijing 100876, China
[2]Department of Electronic Systems, Antennas, Propagation and Millimeter-Wave System (APMS) Section, Aalborg University, 9200 Aalborg, Denmark

Corresponding author: Nan Ma (manan@bupt.edu.cn)

This work was supported by the National Key Research and Development Project of China under Grant 2018YFB2100202.

ABSTRACT Over-the-air (OTA) testing of millimeter-wave (mmWave) adaptive terminal is expected to be an essential step in the product design and development stage. In this paper, we investigated the simple-sectored multi-probe anechoic chamber (SS-MPAC) configuration for testing mmWave adaptive terminal under fading channel conditions. By summarizing the characteristics of the adaptive terminal antenna, four representative antenna sub-arrays were utilized to evaluate the testing performance under two spatial channel models. We also discussed two evaluation metrics to assess the accuracy of the SS-MPAC configuration. The results indicated that, the configuration parameters of SS-MPAC design were determined mainly by the position of the adaptive antenna sub-arrays and the half power beamwidth (HPBW) of adaptive antenna systems. Furthermore, to ensure accurate emulation of spatial correlation between multiple active sub-arrays on the terminal, a much more expensive setup configuration is expected, compared to single active sub-array (single adaptive array, or multiple sub-arrays with switch structure) terminal case. These findings are valuable inputs for the ongoing New Radio (NR) multiple-input multiple-output (MIMO) OTA work in the standardization.

INDEX TERMS Over-the-air testing, mmWave terminal, adaptive terminal, SS-MPAC configuration, beamforming testing.

I. INTRODUCTION

Owing to the rapid growth in wireless data traffic, many new technologies will be developed to enhance fifth-generation (5G) network performance [1]. Among them, the millimeter-wave (mmWave) communications have shown tremendous potential due to the large available contiguous bandwidth. It is being considered by the standardization organization, manufacturers and researchers as the key component to achieve the 5G vision [2], [3].

However, it is generally accepted that the signal-to-interference-plus noise ratio (SINR) reduces considerably owing to high transmission loss and attenuation due to blockage at mmWave bands [3]. To achieve high capacity provided by the large bandwidth, the transceiver systems should offer high signal power to remain good SINR. Therefore, transceiver systems for 5G mmWave devices should incorporate highly directional antennas [4]. Directional antennas with narrow beams (beamforming) and adaptive antenna patterns (beamsteering) are expected. Even though the spatial coverage range can be mitigated by steering the beam, it is still very difficult to achieve full spatial coverage range similar to omnidirectional antennas using one antenna array. Consequently, 5G mmWave devices are anticipated to have multiple antenna arrays (also called sub-arrays) to enable full spherical coverage [5]. These antenna systems contribute to the increasing levels of integration in 5G mmWave devices [5]. A significant consequence of the resulting integration is that traditional radio frequency (RF) connectors at the boundary between the radio distribution network circuit and the antenna system are no longer possible to implement. That is, the connectors are needed for the traditional conducted tests will be no longer available. This change brings great challenges to the development and validation of 5G New Radio (NR), from research and development (R&D) through conformance test, manufacturing and installation and maintenance [6].

Over-the-air (OTA) testing is considered to be feasible approaches [6]–[8]. It has been developed and researched

The associate editor coordinating the review of this manuscript and approving it for publication was Matti Hämäläinen.

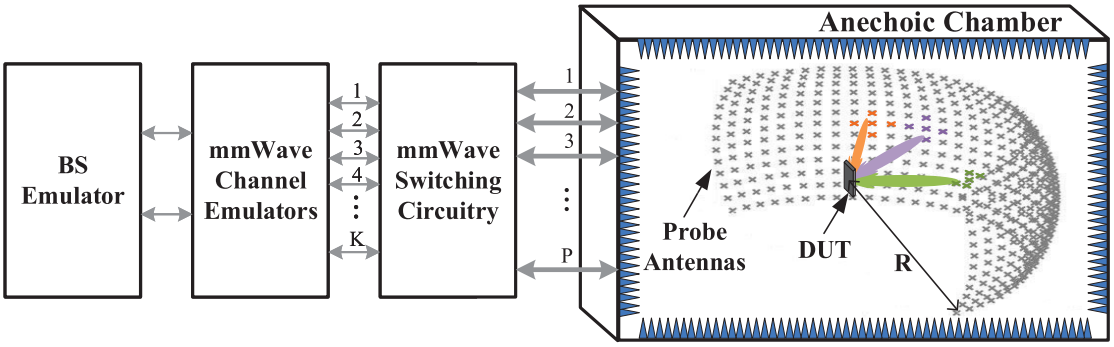

FIGURE 1. An illustration of a SS-MPAC setup.

for many years for sub-6GHz multiple-input multiple-output (MIMO) capable mobile terminals [9]. The purpose of OTA test setups is to generate fading radio-channel conditions around the device under test (DUT) as specified by target channel models. Various OTA methodologies have been proposed for sub-6GHz MIMO DUT, e.g., the reverberation chamber (RC), the multi-probe anechoic chamber (MPAC), and the radiated two-stage (RTS) based method. RC can produce the rich isotropic stochastic environment for DUT. However, since the channel is specular and highly sparse at mmWave frequencies, the method is not appropriate for 5G NR testing. The RTS method has been approved as an alternative Long Term Evolution (LTE) MIMO OTA test method to MPAC in the Third Generation Partnership Project (3GPP) [9]. This method can be useful for static mmWave antenna testing [10], but it will not work for testing under dynamic channel conditions where the DUT antenna pattern is expected to change during the test, since it is not a true end-to-end testing method. MPAC test system defined in 3GPP is well known and widely accepted by the industry for LTE user equipment (UE) MIMO OTA test [9]. It consists of a set of OTA probes evenly spaced in a ring formation, and the DUT placed in the test area in the center of the ring. A uniform probe configuration can offer the flexibility of emulating arbitrary spatial channel profiles [11]. It is straightforward to consider extending the MPAC method to mmWave applications. However, to emulate a 3D higher frequencies environment and a significantly large test area (in wavelength unit), the system might require more than hundreds of probes. This number of probe antennas will bring a huge hardware overhead, which includes many channel emulators (CE) and the size of an anechoic chamber.

To overcome these limitations of current MPAC method, the simple-sectored MPAC (SS-MPAC) method is proposed [12]–[15]. There are several advantages for SS-MPAC based method. The channels in mmWave are well known to be highly sparse and specular. Further, the channel will be filtered by the beamforming operation at the other end of the communication link, leading to more directive channel models seen by the terminal. Therefore, the mmWave channels seen by the terminal will be even more directive. Furthermore, the SS-MPAC with a limited number of active probes has the potential to reduce the total setup costs, including the hardware and the size of the chamber. In the literature, SS-MPAC OTA techniques for mmWave adaptive terminal evaluations have been discussed in [7], [14], [15]. The requirements for the test system design were analyzed in [7], as shown in Fig. 1, including the measurement range R, number of OTA probe antennas, number of active OTA probe antennas, and amount of channel emulator resource. Reference [14] described several metrics to validate system performance for evaluation of mmWave devices, which concentrated more on the beam selection process because of the nature of the DUT antenna type. Based on this, a set of simulations in order to evaluate the setup and to determine the setup configuration parameters, like measurement range length, probe configurations, were conducted in [15].

However, the previous works can be categorized as the "black box" approach, i.e., with no knowledge of the DUT at all, e.g. antenna arrays positions, the operation mode of the DUT. Typically, an antenna array configuration covering the whole terminal form factor is assumed in the black-box approach. Using this approach is overkilling, and may bring up unnecessarily testing system hardware costs. The main reason is that antenna systems can only be placed in several locations of the terminal in few limited area, and its complexity is significantly limited by practical design. In the black box design, the whole DUT is treated as the antenna array, which will never be the case in practice. The alternative approach "white box" is based on prior knowledge of the antenna arrays on the DUT, which is the focus of the paper. Intuitively, the SS-MPAC configuration and complexity can be significantly reduced via utilizing the knowledge of the antenna design in the DUT. This is highly attractive since cost reduction can be achieved. Further, knowledge of DUT antenna systems might be available in development and research stage, via simulation, measurement or specifications.

To address this problem, In this paper, we evaluate the system design for SS-MPAC using the black box and white box approach. In particular, the mmWave UE antenna design features are briefly summarized. According to the different

TABLE 1. Various antenna arrays for 5G adaptive terminal.

# Ref.	[17]	[18]	[19]	[20]	[21]
Antenna element	Patch	Slot	Yagi-Uda	Dipole	Vivaldi
No. of sub-arrays	3	2	4	1	1
Element per sub-array	1×8	8×1	1×16	1×8	1×8
f_0 [GHz]	28	28	28	60	28
HPBW [deg]	12	15	–	16	22
Maximum Gian [dBi]	12.5	15.6	–	12	12
Array position	Top	Left, Right	Four Corners	Top	Top

working modes of UE, we investigate the system configuration under various possible DUT antenna arrays in the white box approach, including single adaptive sub-array, multiple adaptive sub-arrays in switch mode and spatial multiplexing (two sub-arrays working in parallel to transmit/receive two data streams) MIMO. In the end, simulation results are presented.

In Section II, we presented the state-of-art mmWave terminal designs. Section III specifies system models for the radio channel with adaptive antenna sub-array and for the corresponding OTA emulation system. Furthermore, OTA performance metrics for adaptive terminal are described. Simulation settings and results are discussed in Sections IV. Conclusions are outlined in Section VII.

II. STATE-OF-ART MMWAVE TERMINAL DESIGNS

Many proposals for mmWave beam-steerable antennas have been reported in the literature in recent years [16]-[21]. In [20] and [21], single antenna arrays with dipole and Vivaldi antenna elements were presented, respectively. The antenna array at the top of the UEs has a maximum gain of more than 12dBi. The multiple antenna arrays were designed in [17], [18], where the patch and slot antenna element were utilized. Furthermore, in [19], a scheme based on four antenna arrays was investigated. Various antenna arrays are categorized in Table 1. Note that, there are many antennas designs and our list is by no means exhaustive.

As we can see form Table 1, the comparison has been made based on the half power beamwidth (HPBW), maximum gain, antenna element, number of elements on per sub-array, number and position of sub-arrays. These differences all have the potential to affect the system configuration of SS-MPAC. According to this, the mmWave antenna sub-arrays of terminals are used in this paper as follows:

1) Black box, where the antenna array is configured to cover the whole DUT. Consider the DUT size is 160×80 mm, which has a uniform rectangular sub-array with half wavelength spacing between elements. For example, at 28 GHz, the number of antenna elements is about 450.
2) The terminal with one adaptive sub-array. The first kind of model is shown in Fig. 2a, the physical structure of the terminal antenna array is 4×4 as an example. It may be located in different positions or with different antenna elements. Instead, the second model, which ignores the physical structure of the antenna, only considering the HPBW of the terminal.
3) The terminal is equipped with multiple adaptive sub-arrays and operates in switch mode. A diagram of the multiple sub-arrays is shown in Fig. 2b. The subarray1 and subarray2 with the same physical structure and different positions.
4) The terminal is equipped with multiple adaptive sub-arrays and operates in spatial multiplexing mode.

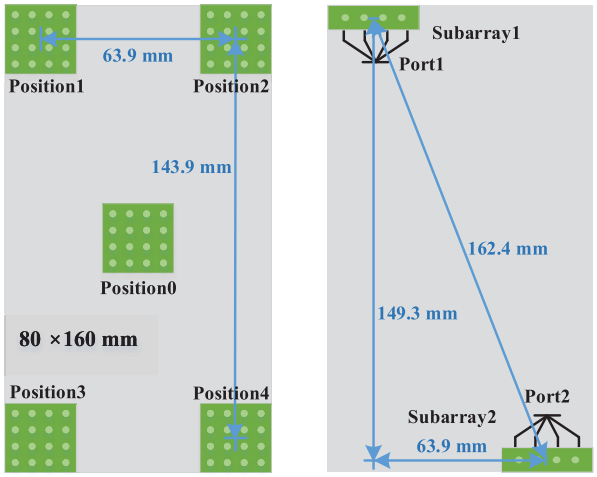

(a) One adaptive sub-array (b) Multiple adaptive sub-arrays

FIGURE 2. A diagram of the mmWave terminal with (a) one adaptive sub-array; (b) multiple adaptive sub-arrays.

Note that the terminal is always located in the center of the test zone, and the antenna sub-arrays all with half wavelength inter-element spacing. Moreover, the antenna element is isotropic, if it is not specified.

III. OTA PERFORMANCE METRIC FOR ADAPTIVE TERMINAL

In this section, we define the signal model for target and SS-MPAC setups. As discussed in Section II, two different evaluation metrics have been discussed for the adaptive terminal, namely beam pattern similarity (BPS) and spatial correlation, as detailed below.

A. SIGNAL MODEL FOR TARGET AND SS-MPAC SETUPS

The signal model for an adaptive terminal with U antenna elements can be written as (neglecting noise)

$$\boldsymbol{Y} = \boldsymbol{W}_{P\times U} \cdot \boldsymbol{H}_{U\times S} \cdot \boldsymbol{X}_{S\times 1} \tag{1}$$

where $\boldsymbol{X}$ is the signal vector radiated by S transmitter antenna elements, $\boldsymbol{H}$ is the channel transfer function from S transmitter antenna elements to U receiver antenna elements on the adaptive terminal. The weight matrix $\boldsymbol{W}$ is designed so as to steer beams to different directions. $\boldsymbol{Y}$ is the signal vector received by P antenna port of adaptive terminal.

For a geometric channel model, the channel transfer function $\boldsymbol{H}$ is defined as

$$\boldsymbol{H}(f,t)=\sum_{n=1}^{N}\boldsymbol{H}_n(f,t) \tag{2}$$

The (u,s)th entry of $\boldsymbol{H}_n(f,t)$ can be expressed as

$$\begin{aligned} &h_{u,s,n}(f,t)\\ &=\sum_{m=1}^{M}\begin{bmatrix} g_u^V(\Omega_{n,m}^{\mathrm{Rx}})\\ g_u^H(\Omega_{n,m}^{\mathrm{Rx}})\end{bmatrix}^T\begin{bmatrix}\chi_{n,m}^{VV} & \chi_{n,m}^{VH}\\ \chi_{n,m}^{HV} & \chi_{n,m}^{HH}\end{bmatrix}\begin{bmatrix} g_s^V(\Omega_{n,m}^{\mathrm{Tx}})\\ g_s^H(\Omega_{n,m}^{\mathrm{Tx}})\end{bmatrix}\\ &\exp(j2\pi\vartheta_{n,m}t+\Phi_{n,m})\exp(-j2\pi f\tau_n)\end{aligned} \tag{3}$$

where $\Omega_{n,m}^{\mathrm{Tx}}$, $\Omega_{n,m}^{\mathrm{Rx}}$, $\vartheta_{n,m}$, $\Phi_{n,m}$ are the angle of departure, angle of arrival, Doppler frequency of mth subpath of the nth cluster, and a random variable following the uniform distribution in $[-\pi,\pi]$, respectively. τ_n is the delay of the nth cluster. g_s^V, g_s^H are the vertically and horizontally polarized field patterns of the sth transmitter antenna element, respectively. Similarity, g_u^V, g_u^H are the vertically and horizontally polarized field patterns of the uth receiver antenna element. Coefficient $\chi_{n,m}^{ab}$ is the complex amplitude of the mth subpath of the nth cluster for transmit polarization b to receive polarization a.

In the OTA case in the SS-MPAC setup illustrated in Fig. 1, the transfer function $\widehat{\boldsymbol{H}}$ is composed by the fading channel emulator and the SS-MPAC setup. $\widehat{\boldsymbol{H}}$ is substituted by

$$\widehat{\boldsymbol{H}}(f,t)=\boldsymbol{F}\cdot\boldsymbol{H}_{\mathrm{OTA}}(f,t) \tag{4}$$

where $\boldsymbol{F}$ is the transfer matrix from K OTA probe antennas to U DUT antennas. In the SS-MPAC system, the transfer function $\boldsymbol{F}$ depends on the OTA probe antennas, free path loss propagation and the antenna characteristics of DUT. $\boldsymbol{H}_{\mathrm{OTA}}(f,t)$ is the second transfer matrix to be executed by channel emulator. The (k,s)th entry for vertically and horizontally polarized of $\boldsymbol{H}_{\mathrm{OTA}}(f,t)$ can be expressed as

$$\begin{aligned} &h_{k,s,n}^{V,\mathrm{OTA}}(f,t)\\ &=\sum_{m}\begin{bmatrix}1\\0\end{bmatrix}^T\begin{bmatrix}\chi_{n,m}^{VV} & \chi_{n,m}^{VH}\\ \chi_{n,m}^{HV} & \chi_{n,m}^{HH}\end{bmatrix}\begin{bmatrix} g_s^V(\Omega_{n,m}^{\mathrm{Tx}})\\ g_s^H(\Omega_{n,m}^{\mathrm{Tx}})\end{bmatrix}\\ &\cdot\exp(j2\pi\vartheta_{n,m}t+\Phi_{n,m})\exp(-j2\pi f\tau_n)\\ &\cdot\sqrt{g_{k,n}}\end{aligned} \tag{5}$$

$$\begin{aligned} &h_{k,s,n}^{H,\mathrm{OTA}}(f,t)\\ &=\sum_{m}\begin{bmatrix}0\\1\end{bmatrix}^T\begin{bmatrix}\chi_{n,m}^{VV} & \chi_{n,m}^{VH}\\ \chi_{n,m}^{HV} & \chi_{n,m}^{HH}\end{bmatrix}\begin{bmatrix} g_s^V(\Omega_{n,m}^{\mathrm{Tx}})\\ g_s^H(\Omega_{n,m}^{\mathrm{Tx}})\end{bmatrix}\\ &\cdot\exp(j2\pi\vartheta_{n,m}t+\Phi_{n,m})\exp(-j2\pi f\tau_n)\\ &\cdot\sqrt{g_{k,n}}\end{aligned} \tag{6}$$

where $g_{k,n}$ is probe power weights of kth OTA probe for nth cluster. It is calculated based on the pre-faded signal synthesis (PFS) technique [15], where the objective is to optimize the power weights for probe antennas to reconstruct the target spatial channel model.

B. OTA METRICS

There is a need for the evaluation metrics to justify how well desired propagation environments are reconstructed by the designed SS-MPAC (i.e. how well $\widehat{\boldsymbol{H}}$ approximates $\boldsymbol{H}$). At mmWave band, the evaluation metrics should emphasize the beamforming performance of the DUT. In this paper, we select the BPS as the metric for the DUT that with one adaptive sub-array. As for multiple adaptive sub-arrays that operate in spatial multiplexing mode, we derive the spatial correlation error between sub-arrays. It is an important metric when multiple signal streams with the sub-arrays are communicated and the polarization domain is not capable to separate the streams.

1) ADAPTIVE ARRAY: BEAM PATTERN SIMILARITY

The metric is to evaluate the similarity of the target and emulated beamforming power pattern as seen by the DUT. The target Bartlett beamforming power pattern can be given as

$$\mathrm{B}(\theta,\phi)=\boldsymbol{\alpha}^H(\theta,\phi)\boldsymbol{R}\boldsymbol{\alpha}(\theta,\phi) \tag{7}$$

where $\boldsymbol{R}\in\mathbb{C}^{U\times U}$ is spatial correlation matrix for the ideal target channel model, (θ,ϕ) is the space angle with θ and ϕ representing elevation and azimuth angle, respectively. $\boldsymbol{\alpha}(\theta,\phi)$ denotes the steering vector of DUT antenna array to the space angle under far-field assumption. $(\cdot)^H$ represents the Hermitian operation, and the u-th entry of $\boldsymbol{\alpha}(\theta,\phi)$ is

$$\begin{aligned}\alpha_u(\theta,\phi)&=e^{-j\boldsymbol{k}\cdot\boldsymbol{r}_u}\\ \boldsymbol{k}&=\frac{2\pi}{\lambda}(\cos\theta\cos\phi,\cos\theta\sin\phi,\sin\theta)\\ \boldsymbol{r}_u&=[x_u,y_u,z_u]^T\end{aligned} \tag{8}$$

where $\boldsymbol{k}$ is the wave vector described by (θ,ϕ), and $\boldsymbol{r}_u$ is the position vector of uth antenna array element on DUT.

The emulated Bartlett beamforming power pattern of the reference channel model by the SS-MPAC setup as

$$\underline{\mathrm{B}}(\theta,\phi)=\boldsymbol{\alpha}^H(\theta,\phi)\underline{\boldsymbol{R}}\boldsymbol{\alpha}(\theta,\phi) \tag{9}$$

where $\underline{\boldsymbol{R}}\in\mathbb{C}^{U\times U}$ is the spatial correlation function achievable with a SS-MPAC setup.

The similarity of the beamforming power patterns with target and emulated is defined as

$$\mathrm{S}=(1-\mathrm{D_P})\times 100\% \tag{10}$$

The range of S is [0, 1], where zero denotes maximal dissimilarity and one full similarity. $\mathrm{D_P}$ is the pattern distortion factor, which can be defined as

$$\mathrm{D_p}=\frac{1}{2}\iint\left|\frac{\mathrm{B}(\theta,\phi)}{\iint\mathrm{B}(\theta',\phi')\mathrm{d}\theta'\mathrm{d}\phi'}-\frac{\underline{\mathrm{B}}(\theta,\phi)}{\iint\underline{\mathrm{B}}(\theta',\phi')\mathrm{d}\theta'\mathrm{d}\phi'}\right|\mathrm{d}\theta\mathrm{d}\phi \tag{11}$$

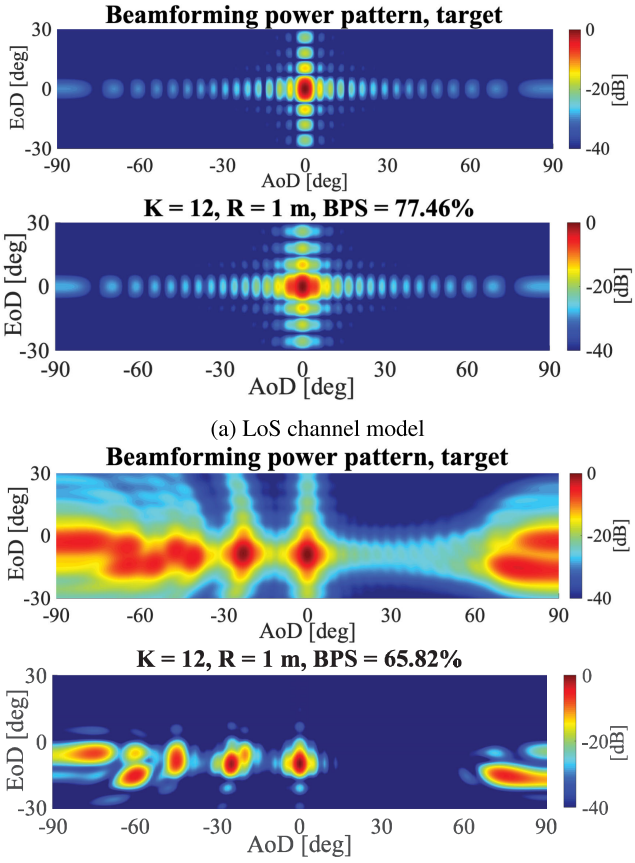

(a) LoS channel model

(b) CDL-C channel model

FIGURE 3. The target and OTA beamforming power pattern of black box with (a) LoS channel; (b) CDL-C channel model.

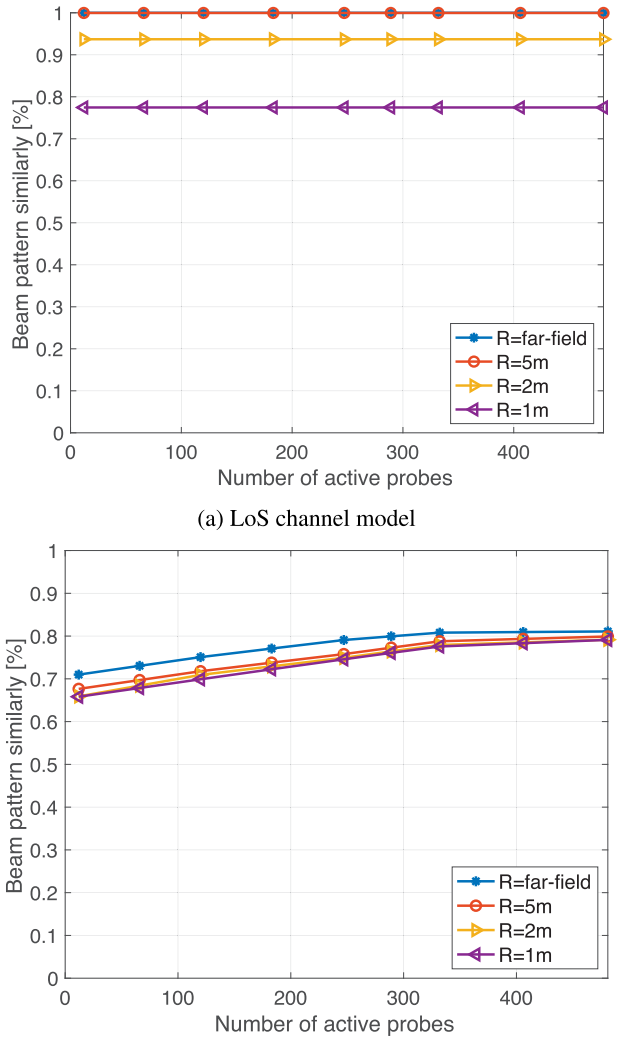

(a) LoS channel model

(b) CDL-C channel model

FIGURE 4. Beam pattern similarity as a function of active probe numbers with $R = 1$ m, $R = 2$ m, $R = 5$ m and far-field of black box under (a) LoS channel model; (b) CDL-C channel model.

2) SPATIAL MULTIPLEXING: SPATIAL CORRELATION

In LTE MPAC setup system, the spatial correlation is generally considered as the correlation of signals received by antenna elements within test area. However, in order to investigate the SS-MPAC setup configuration on testing of DUT that operates in spatial multiplexing mode, we consider the correlation of signals received and integrated by DUT antenna sub-arrays [22]. Suppose that the signals form the antenna elements are multiplied by a complex weight vector and then summed together to from the received signal by each antenna sub-array. The sub-arrays are steered to the boresight direction in this paper. The intention of this metric is to evaluate the impact of the limited SS-MPAC setup configuration on OTA testing of radio devices with multiple antenna sub-arrays, such as limited range length and number of active probes.

The target case is when the range length between the DUT antenna arrays and the probe antennas meets the far-field. As shown in Fig. 2b, there are two sub-arrays on the DUT as an example, and the number of elements in subarray1 and subarray2 is Q and V, respectively. The array factor of subarray1 and subarray2 to the kth probe antenna direction (θ_k, ϕ_k) are

$$A_1(\theta_k, \phi_k) = \sum_{q=1}^{Q} \omega_q^{'} \alpha_q(\theta_k, \phi_k)$$
$$A_2(\theta_k, \phi_k) = \sum_{v=1}^{V} \omega_v^{''} \alpha_v(\theta_k, \phi_k) \quad (12)$$

where $\boldsymbol{\alpha}$ is the steering vector of sub-array as in (8), $\boldsymbol{\omega}^{'}$ and $\boldsymbol{\omega}^{''}$ is the complex weight vector of subarray1 and subarray2, respectively. In particular, when the positions of the two arrays on DUT are fixed, the beams of the sub-arrays depend entirely on their complex weight vector.

Then, the covariance of combined signals can be written as

$$C_{12} = \sum_{k=1}^{K} (\sqrt{g_k} \cdot A_1(\theta_k, \phi_k)) \cdot (\sqrt{g_k} \cdot A_2(\theta_k, \phi_k))^* \quad (13)$$

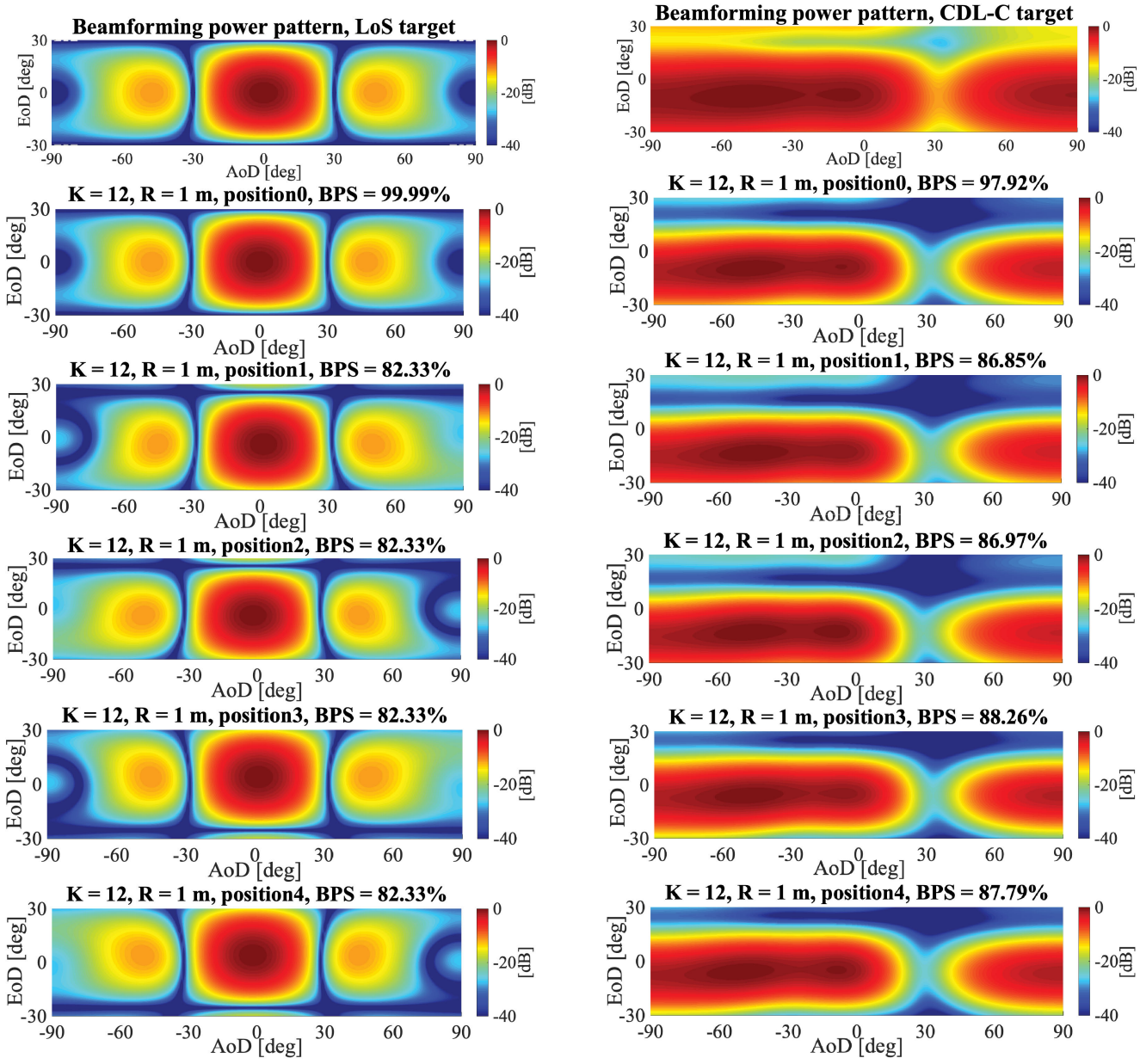

(a) LoS channel model (b) CDL-C channel model

FIGURE 5. The target and OTA beamforming power pattern of 4 × 4 isotropic antenna sub-array with (a) LoS channel; (b) CDL-C channel model.

where g_k is the probe power weight of kth probe antennas, which can be obtained from the PFS technique [15] with target spatial channel model. $(\cdot)^*$ represents the complex conjugate operation.

The auto-covariance of subarray1 and subarray2 are

$$C_{11} = \sum_{k=1}^{K} (\sqrt{g_k} \cdot A_1(\theta_k, \phi_k)) \cdot (\sqrt{g_k} \cdot A_1(\theta_k, \phi_k))^*$$

$$C_{22} = \sum_{k=1}^{K} (\sqrt{g_k} \cdot A_2(\theta_k, \phi_k)) \cdot (\sqrt{g_k} \cdot A_2(\theta_k, \phi_k))^* \quad (14)$$

Then the spatial correlation of target case is

$$\rho_{far} = \frac{C_{12}}{\sqrt{C_{11} C_{22}}} \quad (15)$$

As in limited range length case, i.e. near-field, the transfer function of subarray1 and subarray2 to the kth probe antenna direction (θ_k, ϕ_k) are

$$\underline{A}_1(\theta_k, \phi_k) = \sum_{q=1}^{Q} \omega_q' \sqrt{L(d_{q,k})} \cdot e^{j\frac{2\pi}{\lambda} d_{q,k}}$$

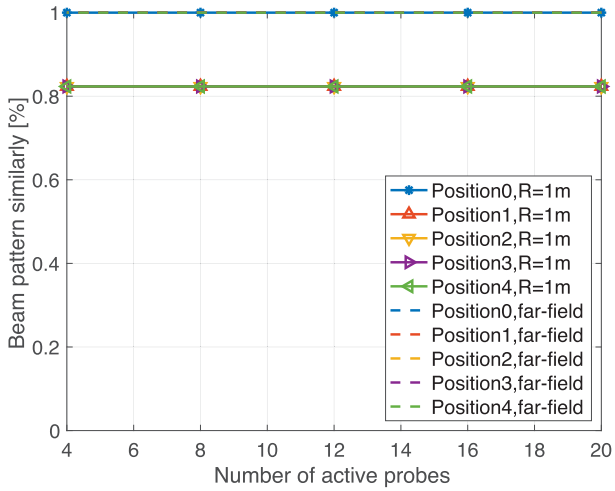

(a) LoS channel model

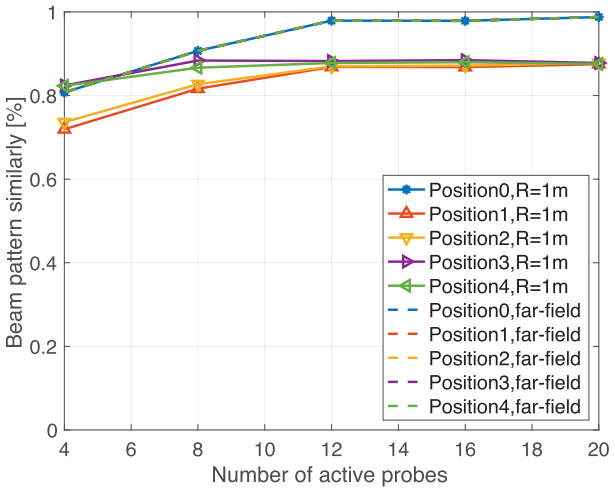

(b) CDL-C channel model

FIGURE 6. Beam pattern similarity as a function of active probe numbers with $R = 1$ m, far-field and different positions of antenna sub-array under (a) LoS channel model; (b) CDL-C channel model.

$$\underline{A}_2(\theta_k, \phi_k) = \sum_{v=1}^{V} \omega_v'' \sqrt{L(d_{v,k})} \cdot e^{j\frac{2\pi}{\lambda} d_{v,k}} \tag{16}$$

where $L(\cdot)$ is the path loss term, $d_{q,k}$ and $d_{v,k}$ is the distance from the kth OTA probe antenna to the qth antenna element in subarray1 and vth antenna element in subarray2, respectively. λ is the wavelength.

Similarly, using $\underline{A}_1$ and $\underline{A}_2$ in (16) instead of A_1 and A_2 in (13) and (14), we can get the covariance matrix $\underline{C}_{12}$ and auto-covariance matrix $\underline{C}_{11}, \underline{C}_{22}$ in limited range length case. Therefore, the spatial correlation in the near-field case is

$$\rho_{near} = \frac{\underline{C}_{12}}{\sqrt{\underline{C}_{11}\underline{C}_{22}}} \tag{17}$$

Finally, the spatial correlation error with the far-field and near-field can be calculated as

$$\rho_{error} = \left| \rho_{far} - \rho_{near} \right| \tag{18}$$

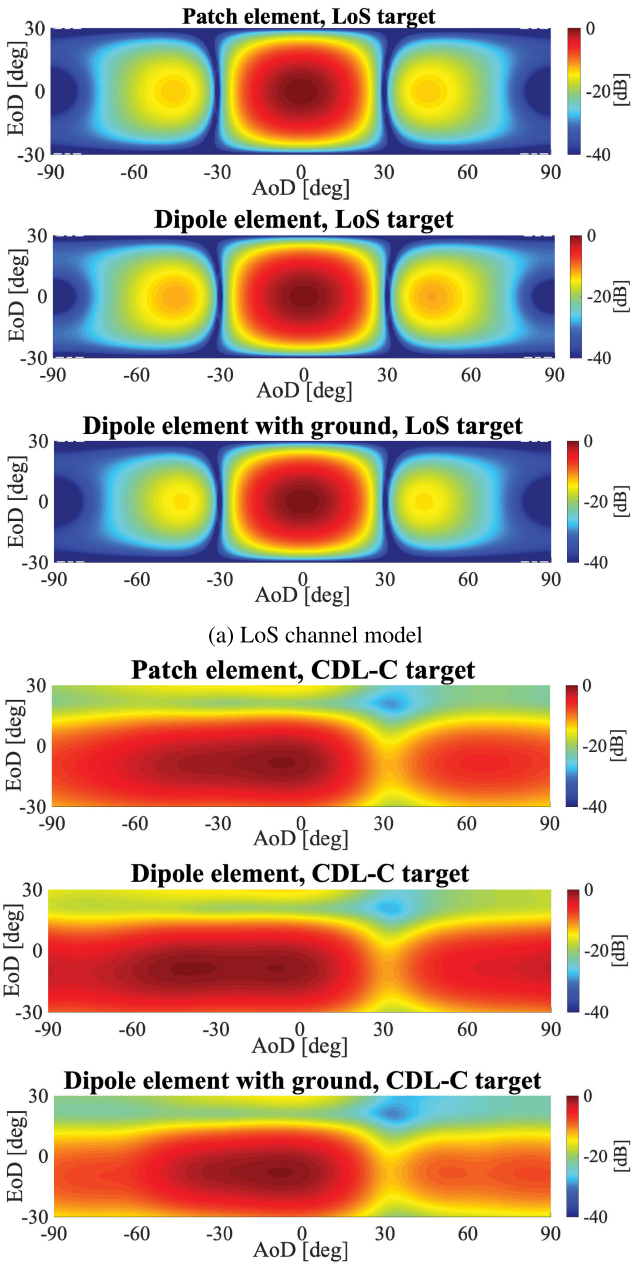

(a) LoS channel model

(b) CDL-C channel model

FIGURE 7. The target and OTA beamforming power pattern of 4 × 4 sub-array with different antenna elements under (a) LoS channel; (b) CDL-C channel model.

In the following simulation, the impact of the limited range length and number of active probes on spatial correlation error will be simulated.

IV. SIMULATION RESULTS

A. TARGET CHANNEL MODELS

The simulation system follows the description in Section III. A large set of OTA probe antennas is located on the sector angle of interest and with the same distance (range length) R to the center of the DUT. We fix certain parameters

to reduce the independent variables in the simulation. The angular region for the sector of interest is $[-90°, 90°]$ and $[-30°, 30°]$ in azimuth and elevation, respectively. A sampling density of 5° in the azimuth and elevation domain is utilized. Therefore, the number of probes in the azimuth domain is $\frac{180}{5} + 1 = 37$, and that in the elevation domain is $\frac{60}{5} + 1 = 13$. The total number of probes in the system is $37 \times 13 = 481$. A line of sight (LoS) and a non-line of sight (NLoS) channel model CDL-C specified in [23] are simulated at $f = 28$ GHz as examples, without any scaling in the angular or delay domain. Only the clusters falling into the angular sector of interest are considered here.

B. SIMULATION RESULTS

To visualize the impact of the mmWave adaptive terminal on the SS-MPAC design, we consider two important configuration parameters of design, i.e., the number of active probes and measurement range length. We show the simulated metrics for the combinations of terminal and channel models, with different numbers of active probes and limited range length. Here, the active probes are the ones that can be simultaneously used in synthesizing the radio channels. In the simulation, we select K dominant probes from the available 481 probe antennas, which are obtained through the PFS technique and probe selection algorithm [12].

The distance $R = 1000$ m is taken as the reference case, in which no near-field effects are present, i.e., far-field. In each of the terminal model, two diagrams are shown as follows: Figs. 3, 5, 7, and 9, and 12 are the target and OTA beamforming power pattern with two channel models, and Figs. 4, 6, 8, 10, 11, 13, and 14 show the metrics as a function of the number of active probes and range length with two channel models.

1) BLACK BOX

The beamforming power patterns under the LoS and CDL-C channel model are shown in Fig. 3a and Fig. 3b, respectively. In each of the figures, top is the target, and bottom is the emulated results in SS-MPAC. Compared with the target result effect, the emulated result effect is nonideal when the number of probes $K = 12$ and range length $R = 1$ m. Fig. 4 shows the effect of active probe number and measurement range length on BPS. With the LoS channel model, the BPS depends on range length because only one probe at the boresight direction is used. On the contrary, the range length has no remarkable effect on the BPS with the CDL-C channel model, but it mainly depends on the number of active probes. Fig. 4b depicts that the BPS is only 81.08% when all probes are switched. The total number of probes in this simulation is 481. If the sampling density of the probe is smaller than 5° in the angular region for the sector of interest, that is, the total number of probes is larger, then the emulated results of the black box in SS-MPAC will be improved.

For the black box, the measurement range length of $R = 5$ m is sufficient, and the number of active probes is more than 481 for all simulated channel models. This number is unpractical for the system configuration. Note that the black box DUT is typically assumed in the literature. In the following, we discussed the system configuration for white box DUT scenarios, which is also the main contribution of the paper.

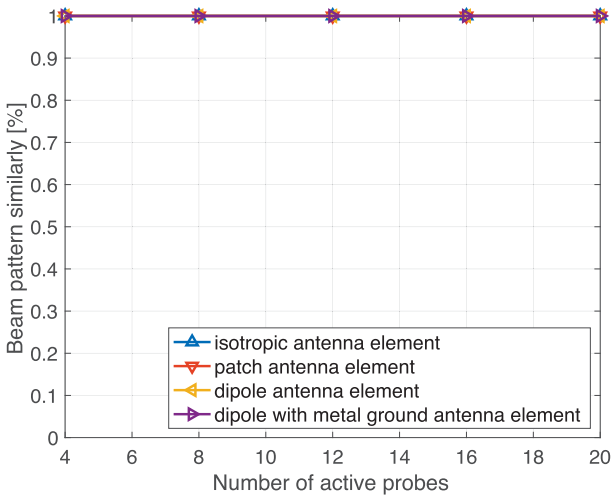

(a) LoS channel model

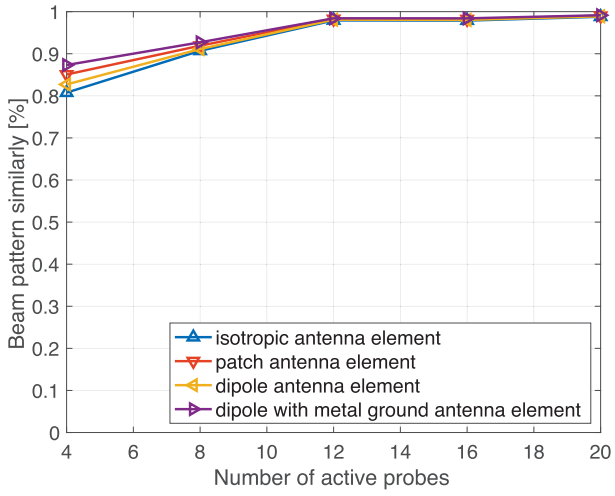

(b) CDL-C channel model

FIGURE 8. Beam pattern similarity as a function of active probe numbers with different antenna elements under (a) LoS channel model; (b) CDL-C channel model.

2) THE TERMINAL WITH ONE ADAPTIVE SUB-ARRAY

The isotropic 4×4 antenna array with half wavelength inter-element spacing at different positions is used to determine the metric of BPS. The positions of each sub-array are specified in Fig. 2a. The sub-array at position0 is always in the center of the coordinate system as a reference. The target and OTA beamforming power patterns are shown in Fig. 5. For the OTA case, the number of active probes is set to 12 as a reference. The beamforming power patterns of positions0-4 are different from the target one with both channel models. In the LoS case,

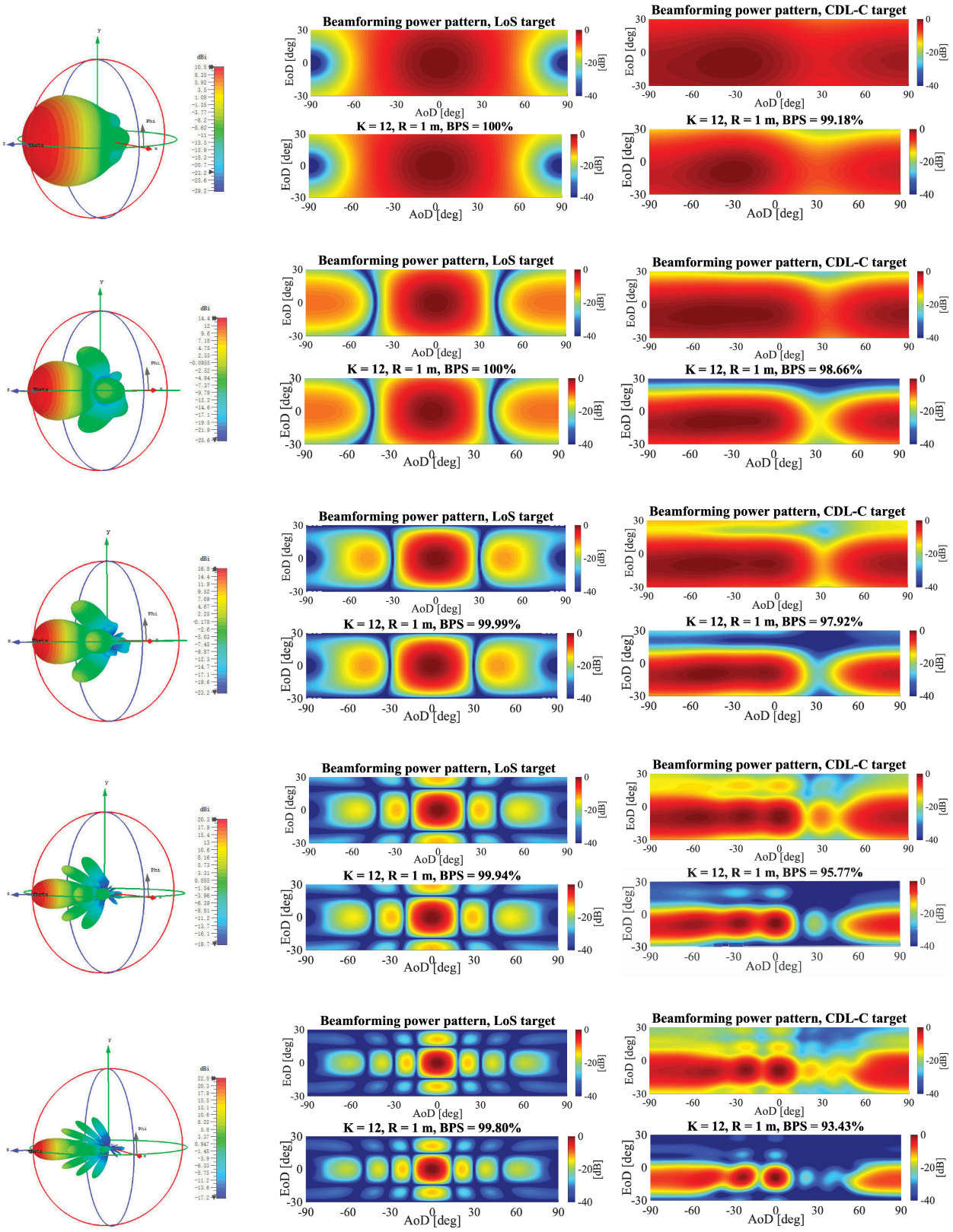

FIGURE 9. Antenna radiation pattern, the target and OTA beamforming power pattern with different HPBWs under LoS and CDL-C channel model.

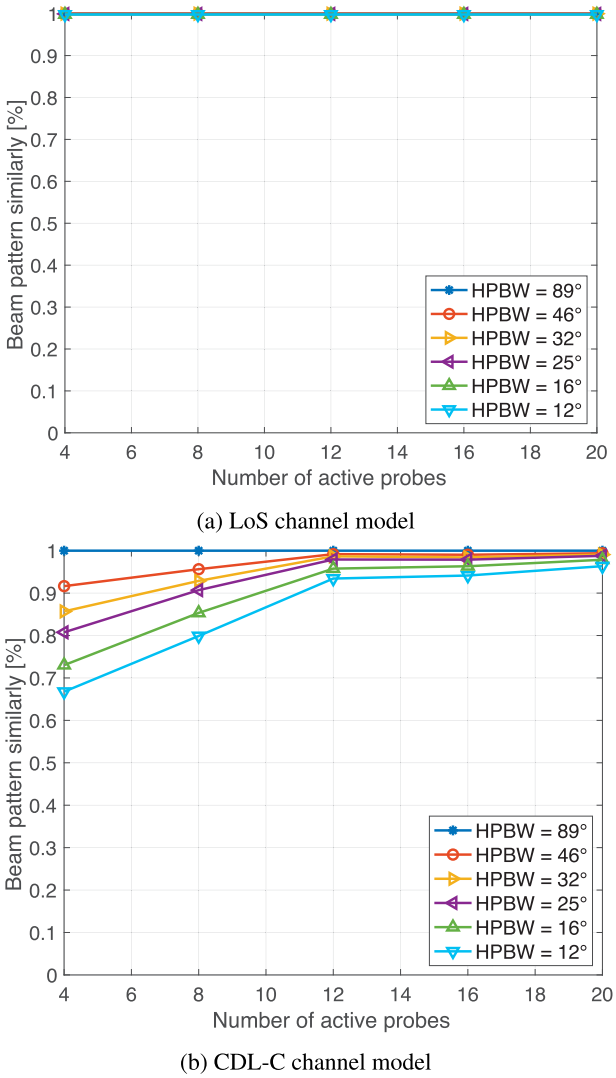

(a) LoS channel model

(b) CDL-C channel model

FIGURE 10. Beam pattern similarity as a function of active probe numbers with different HPBWs under (a) LoS channel model; (b) CDL-C channel model.

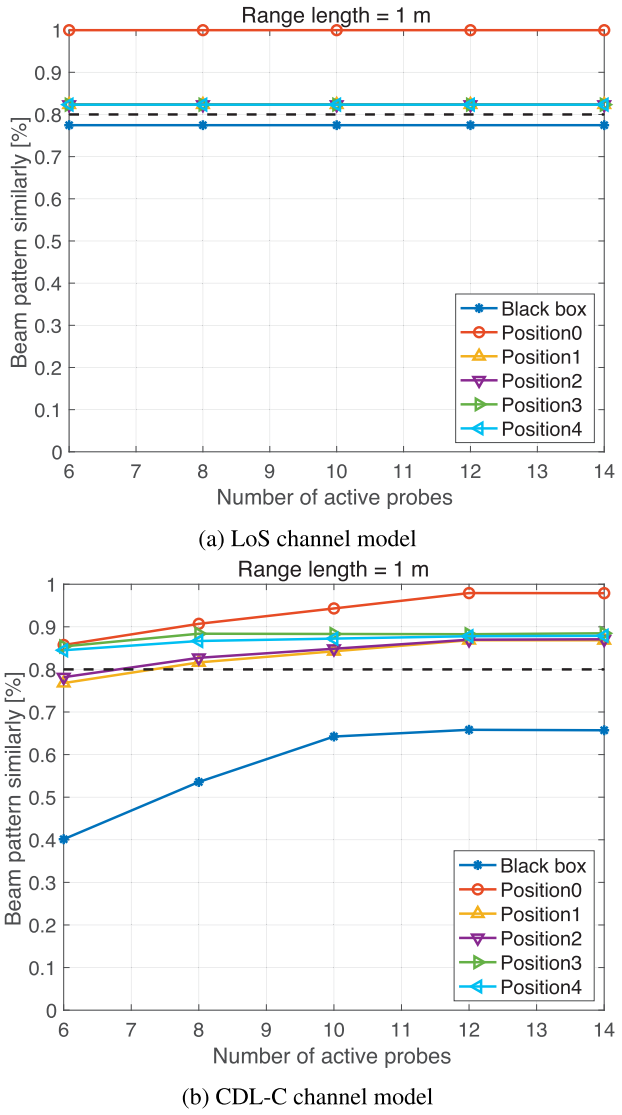

(a) LoS channel model

(b) CDL-C channel model

FIGURE 11. Beam pattern similarity as a function of active probe numbers with different black box and white box under (a) LoS channel model; (b) CDL-C channel model.

only one probe at the boresight direction is used. Owing to the symmetry of the DUT, the results of position1-4 are the same. However, they are different from the results of position0 due to the limitation of measurement range length. As for the CDL-C channel model, the target power azimuth spectrum is discretized by the active probes. Therefore, the difference between the results of position0 and the target is due to the limited range length and insufficient number of active probes. The range length limit also increases the error of positions1-4.

For both channel models, the BPS of position0 is over 97%. Although the position deviation of positions1-4 reduces the BPS, it can still reach more than 80%. Positions1-4 are the most extreme case on DUT. In brief, the measurement range length of $R = 1$ m is sufficient with all simulated channel models in this one adaptive sub-array. In the following simulations, we mainly analyze the simulation effects when $R = 1$ m and with far-field.

The diagrams in Fig. 6 illustrate how the BPS changes with the number of active probes and different antenna array locations in the range length of 1 m and with far-field. Fig. 6a shows that the BPS is the same for all active probe numbers in the LoS channel model, because only one probe at the boresight direction is used. For the CDL-C model, as shown in Fig. 6b, the difference between the curves is due to the limited number of active probes and range length. The increased active probe number has a positive effect on the BPS, but it is almost saturated after 12 probes. The results in different locations are almost the same in the far-field and $R = 1$ m. Therefore, the position deviation of the antenna sub-array should reduce the BPS unless the far-field criterion is fulfilled.

Fig. 7 shows the beamforming power pattern of the 4×4 antenna sub-array with different antenna elements. The

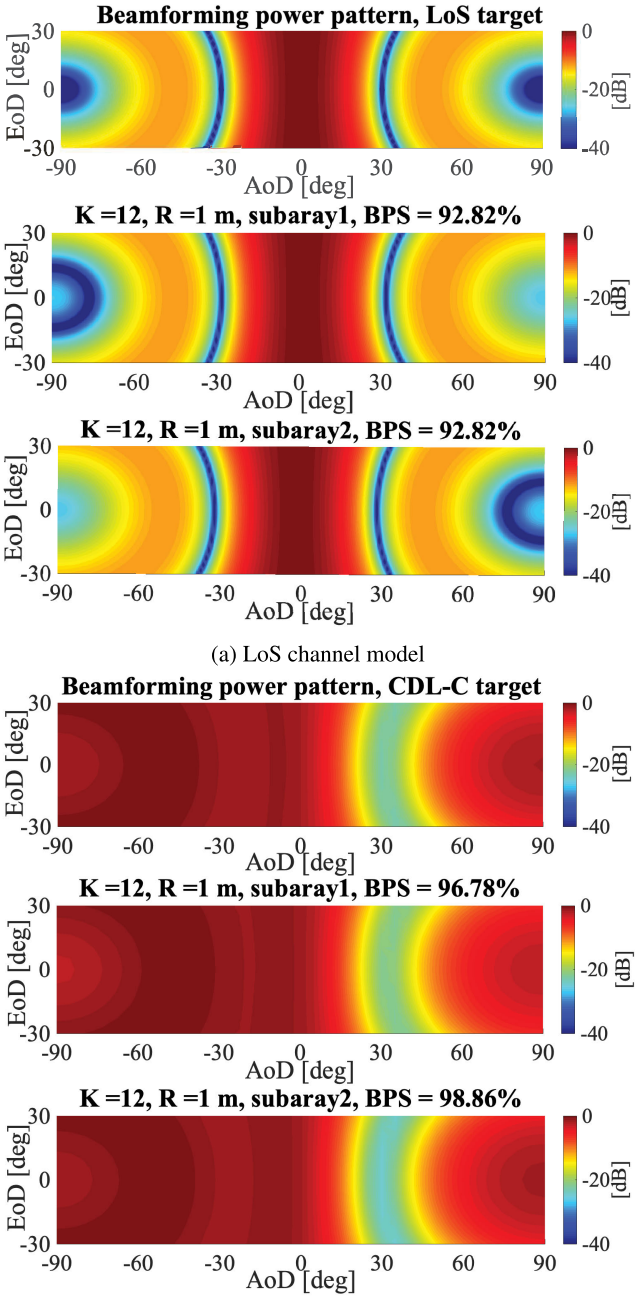

(a) LoS channel model

(b) CDL-C channel model

FIGURE 12. The target and OTA beamforming power pattern of subarray1 and subarray2 under (a) LoS channel; (b) CDL-C channel model.

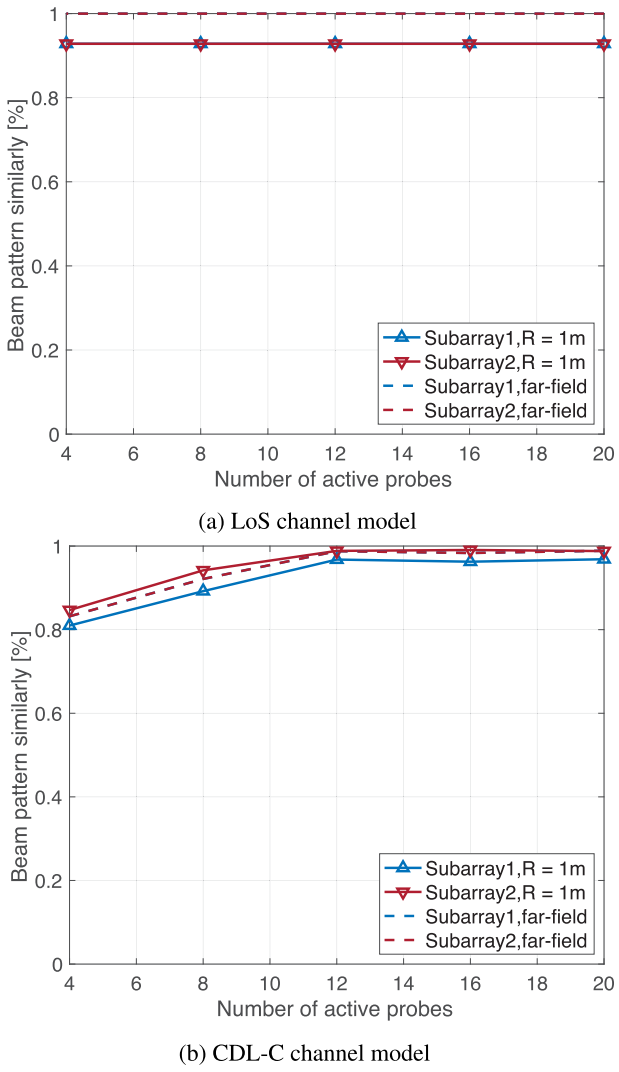

(a) LoS channel model

(b) CDL-C channel model

FIGURE 13. Beam pattern similarity as a function of active probe numbers with $R = 1$ m, far-field, subarray1 and subarray2 under (a) LoS channel model; (b) CDL-C channel model.

antenna sub-array is placed in position0. Three common antenna elements, namely, patch, dipole, and dipole with ground plane, are used in this simulation. For each channel model, the target beamforming power patterns with different antenna elements are almost the same as the isotropic antenna sub-array shown in Fig. 5. A similar conclusion can be drawn from the performance simulation in Fig. 8, and the difference among the beam pattern similarities of different antenna elements is small. The influence of antenna elements on BPS can be negligible.

The DUT radiation patterns of different HPBWs, which ignore the physical structure of the antenna, are shown in Fig. 9 (left). The order of HPBWs in Fig. 9 (left) from top to bottom is 46°, 32°, 25°, 16°, and 12°. Fig. 9 (right) depicts the corresponding target and OTA beamforming power pattern of the two channel models. The narrower the HPBW of DUT, the higher the DUT beam resolution. Fig. 10 shows how the metric changes with the different numbers of active probes and HPBWs. As for the LoS model, only a small difference exists among HPBWs, and no difference exists in the number of active probes. With the CDL-C model, however, the BPS of different HPBWs is different, it decreases with a decrease in HPBW and increases with an increase in the number of active probes. As the number of active probes increases, the metric difference among different HPBWs is reduced.

The 3GPP co-existence studies in [24] assume the HPBW of UE is 25°, although practical HPBW of UE may be a

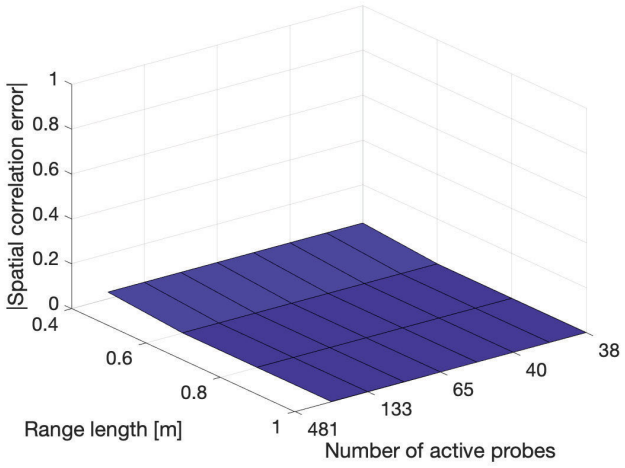

(a) LoS channel model

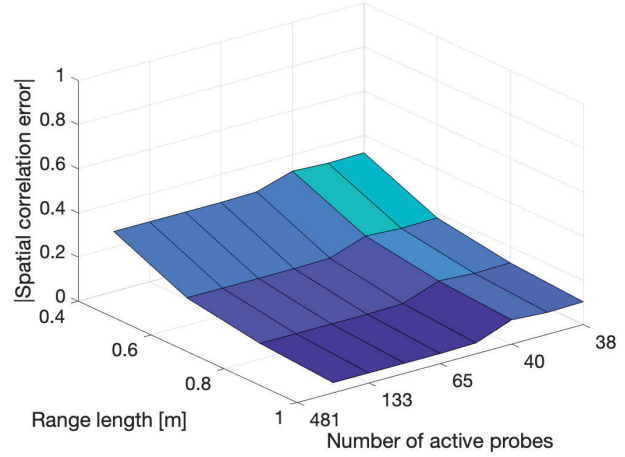

(b) CDL-C channel model

FIGURE 14. Spatial correlation error with two sub-array as a function of active probe numbers and range length with (a) LoS channel model; (b) CDL-C channel model.

lot wider. Therefore, for the terminal with one adaptive sub-array, the isotropic 4×4 antenna arrays with different positions are used to compare with the black box model. As shown in Fig. 11, the measurement range length of $R = 1$ m and the number of active probes $K = 8$ are sufficient with all simulated channel models in white box mode. Compared with the black box mode, the white box mode can greatly reduce the total SS-MPAC setup cost, including the hardware and the size of the chamber.

3) THE TERMINAL IS EQUIPPED WITH MULTIPLE ADAPTIVE SUB-ARRAYS AND OPERATES IN SWITCH MODE

As shown in Fig. 2b, the antenna elements are divided into two sub-arrays, i.e., subarrays1 and subarray2. The elements in each sub-array are combined into a single RF port by an analog weighting matrix. The matrix enables the composition of a set of predefined antenna beams. Thus, the antenna elements fed by the RF port comprise several sub-arrays to enable great spherical coverage.

The target and OTA beamforming power patterns of each sub-array with two channel models are shown in Fig. 12. The results of subarrays1 and subarrays2 are different with that of the target due to the limited range length. For the CDL-C case, the difference is also due to the limited number of active probes. The diagrams in Fig. 13 illustrate how the beam pattern similarities of subarrays1 and subarrays2 change with the number of active probes in $R = 1$ m and in the far-field. Similar to the previous simulation results, in the LoS case, those of subarrays1 and subarrays2 are the same in $R = 1$ m and in the far-field, respectively. As for the CDL-C case, the difference among the curves is due to the limited number of active probes and range length at the beginning. When sufficient probes are available, the difference is only affected by the range length.

4) THE TERMINAL IS EQUIPPED WITH MULTIPLE ADAPTIVE SUB-ARRAYS AND OPERATES IN SPATIAL MULTIPLEXING MODE

When DUT operates in the spatial multiplexing mode, the spatial correlation error is used as an evaluation metric. As shown in Fig. 2b, the distance between subarrays1 and subarray2 is 162.4 mm for reference. The spatial correlation coefficient in (18) is calculated for range lengths R and the number of active probes. The effect of varying parameters on the correlation error for sub-arrays is illustrated in Fig. 14. The error increases with a decrease in R. Particularly, the error increases rapidly as the range length decreases with the CDL-C model. The range length should be greater than 0.8 m, and the number of active probes should not be less than 38 to ensure that the spatial correlation error is less than 0.1. The channel model has a great influence on spatial correlation error in the same setup configuration. If the target channel model is highly spread and has numerous equally strong clusters, then the setup requires additional active probes and a large range length to ensure the spatial correlation of the two sub-arrays.

V. CONCLUSION

The previous works of SS-MPAC design have treated the DUT as a black box. Using this approach is overkilling, and may bring up unnecessarily testing system hardware costs. Moreover, the antenna system can only be placed in a several locations of the terminal due to the available area and design limitations of terminal. In this paper, we have discussed the SS-MPAC design in white box approach. Considering the type of antenna system, the mmWave adaptive terminal was divided into four cases: black box, the terminal with one adaptive sub-array, the terminal equipped with multiple adaptive sub-arrays and operates in the switch mode, and the terminal equipped with multiple adaptive sub-arrays and operates in the spatial multiplexing mode. We have also discussed two metrics and conducted a set of simulations to evaluate the configuration parameters of the SS-MPAC design in different cases.

The simulation results demonstrated that the position of the antenna sub-array and the HPBW of the terminal have a great influence on the SS-MPAC design, but the antenna elements showed a minimal influence. For the terminal with one antenna port and the HPBW of the sub-array is wider than 25°, the found recommended that the measurement range length of $R = 1$ m and the number of active probes $K = 8$ are sufficient with all simulated channel models. Compared with the black box mode, the white box mode that with one antenna port can greatly reduce the total SS-MPAC setup cost, including the hardware and the size of the chamber. As for multiple sub-arrays operating in the spatial multiplexing mode, the spatial correlation error mainly depended on channel models. For each channel model, the error increased with a decrease in range length and number of active probes. The recommended configuration parameters for the adaptive terminal with two 1×4 antenna sub-arrays in the CDL-C channel model are $K \geq 38$ and $R \geq 0.8$. In this case, it does not significantly reduce the cost of the testing system.

Qualitative analysis was applied to the SS-MPAC design for the mmWave adaptive terminal. For future work, the emulator realizable of SS-MPAC should be investigated using standard channel models that combine space, time, and frequency characteristics. Calibration procedures for a practical SS-MPAC system might be challenging at mmWave frequencies and may require further investigation.

ACKNOWLEDGMENT

The authors would like to thank the help and discussions from Mr. P. Mei, Mr. Y. Ji and Mrs. G. Zhang with Aalborg University.

REFERENCES

[1] C.-X. Wang, F. Haider, X. Gao, X.-H. You, Y. Yang, D. Yuan, H. Aggoune, H. Haas, S. Fletcher, and E. Hepsaydir, "Cellular architecture and key technologies for 5G wireless communication networks," *IEEE Commun. Mag.*, vol. 52, no. 2, pp. 122–130, Feb. 2014.

[2] T. S. Rappaport, S. Sun, R. Mayzus, H. Zhao, Y. Azar, K. Wang, G. N. Wong, J. K. Schulz, M. Samimi, and F. Gutierrez, "Millimeter wave mobile communications for 5G cellular: It will work!" *IEEE Access*, vol. 1, pp. 335–349, 2013.

[3] T. S. Rappaport, Y. Xing, G. R. Maccartney, A. F. Molisch, E. Mellios, and J. Zhang, "Overview of millimeter wave communications for fifth-generation (5G) wireless networks—With a focus on propagation models," *IEEE Trans. Antennas Propag.*, vol. 65, no. 12, pp. 6213–6230, Dec. 2017.

[4] D. Liu, W. Hong, T. S. Rappaport, C. Luxey, and W. Hong, "What will 5G antennas and propagation be?" *IEEE Trans. Antennas Propag.*, vol. 65, no. 12, pp. 6205–6212, Dec. 2017.

[5] W. Hong, K.-H. Baek, and S. Ko, "Millimeter-wave 5G antennas for smartphones: Overview and experimental demonstration," *IEEE Trans. Antennas Propag.*, vol. 65, no. 12, pp. 6250–6261, Dec. 2017.

[6] M. Rumney, P. Kyösti, and J. Kyröläinen, "The need for spatial channel emulation to evaluate mmwave UE and base station performance," in *Proc. 12th Eur. Conf. Antennas Propag. (EuCAP)*, 2018, p. 5.

[7] W. Fan, P. Kyosti, M. Rumney, X. Chen, and G. F. Pedersen, "Over-the-air radiated testing of millimeter-wave beam-steerable devices in a cost-effective measurement setup," *IEEE Commun. Mag.*, vol. 56, no. 7, pp. 64–71, Jul. 2018.

[8] P. Zhang, X. Yang, J. Chen, and Y. Huang, "A survey of testing for 5G: Solutions, opportunities, and challenges," *China Commun.*, vol. 16, no. 1, pp. 69–85, Jan. 2019.

[9] *Verification of Radiated Multi-Antenna Reception Performance of User Equipment (UE)*, document TR 37.977, V15.0.0, Sep. 2018.

[10] Y. Jing, M. Rumney, H. Kong, and Z. Wen, "Overview of 5G UE OTA performance test challenges and methods," in *IEEE MTT-S Int. Microw. Symp. Dig.*, May 2018, pp. 1–4.

[11] A. Khatun, T. Laitinen, V.-M. Kolmonen, and P. Vainikainen, "Dependence of error level on the number of probes in over-the-air multiprobe test systems," *Int. J. Antennas Propag.*, vol. 2012, pp. 1–6, Mar. 2012.

[12] P. Kyosti, W. Fan, G. F. Pedersen, and M. Latva-Aho, "On dimensions of OTA setups for massive MIMO base stations radiated testing," *IEEE Access*, vol. 4, pp. 5971–5981, 2016.

[13] W. Fan, I. Carton, P. Kyosti, A. Karstensen, T. Jamsa, M. Gustafsson, and G. F. Pedersen, "A step toward 5G in 2020: Low-cost OTA performance evaluation of massive MIMO base stations," *IEEE Antennas Propag. Mag.*, vol. 59, no. 1, pp. 38–47, Feb. 2017.

[14] A. Hekkala, P. Kyosti, J. Kyrolainen, L. Hentila, and W. Fan, "Performance evaluation of sectored MPAC for 5G UE antenna systems," in *Proc. 6th Asia–Pacific Conf. Antennas Propag. (APCAP)*, Oct. 2017, pp. 1–3.

[15] P. Kyosti, L. Hentila, W. Fan, J. Lehtomaki, and M. Latva-Aho, "On radiated performance evaluation of massive MIMO devices in multiprobe anechoic chamber OTA setups," *IEEE Trans. Antennas Propag.*, vol. 66, no. 10, pp. 5485–5497, Oct. 2018.

[16] A. Naqvi and S. Lim, "Review of recent phased arrays for millimeter-wave wireless communication," *Sensors*, vol. 18, no. 10, p. 3194, Sep. 2018.

[17] N. Ojaroudiparchin, M. Shen, S. Zhang, and G. F. Pedersen, "A switchable 3-D-coverage-phased array antenna package for 5G mobile terminals," *IEEE Antennas Wireless Propag. Lett.*, vol. 15, pp. 1747–1750, 2016.

[18] B. Yu, K. Yang, C.-Y.-D. Sim, and G. Yang, "A novel 28 GHz beam steering array for 5G mobile device with metallic casing application," *IEEE Trans. Antennas Propag.*, vol. 66, no. 1, pp. 462–466, Jan. 2018.

[19] W. Hong, S.-T. Ko, Y. Lee, and K.-H. Baek, "Multi-polarized antenna array configuration for mmWave 5G mobile terminals," in *Proc. Int. Workshop Antenna Technol. (iWAT)*, Mar. 2015.

[20] Y. Li and K.-M. Luk, "A multibeam end-fire magnetoelectric dipole antenna array for millimeter-wave applications," *IEEE Trans. Antennas Propag.*, vol. 64, no. 7, pp. 2894–2904, Jul. 2016.

[21] N. Ojaroudiparchin, M. Shen, and G. F. Pedersen, "Design of Vivaldi antenna array with end-fire beam steering function for 5G mobile terminals," in *Proc. 23rd Telecommun. Forum Telfor (TELFOR)*, Nov. 2015, pp. 587–590.

[22] P. Kyösti, *Some Considerations on Correlations of Hybrid Beamforming Arrays in the Context of OTA Testing*, document TD(19)10058, Oulu, Finland, May 2019.

[23] *Study on Channel Model for Frequencies from 0.5 to 100 GHz*, document TR 38.901, V15.0.0, Jan. 2018.

[24] *Study on New Radio Access Technology: Radio Frequency (RF) and Co-Existence Aspect*, document TR 38.803, v14.2.0, Sep. 2017.

XIAOLI YANG received the B.E. degree in electronics and information engineering from Hubei University, Wuhan, China, in 2009. She is currently pursuing the Ph.D. degree in information and communication engineering with BUPT. Her research interests include channel modeling and over-the-air testing of multiple antenna systems.

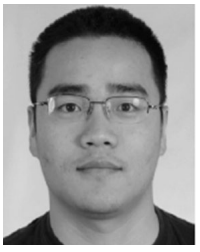

WEI FAN received the B.E. degree from the Harbin Institute of Technology, China, in 2009, the master's double degree (Hons.) from the Politecnico di Torino, Italy, and the Grenoble Institute of Technology, France, in 2011, and the Ph.D. degree from Aalborg University, Denmark, in 2014. In 2011, he was a Research Intern with Intel Mobile Communications, Denmark. He is currently an Associate Professor with the Antennas, Propagation, and Millimeter-Wave Systems Section, Aalborg University. He conducted a three-month internship at Anite Telecoms Oy, Finland, in 2014. His main areas of research are over the air testing of multiple antenna systems, radio channel sounding, modeling, and emulation.

NAN MA received the B.S. and Ph.D. degrees from the Beijing University of Posts and Telecommunications (BUPT), China, in 2002 and 2007, respectively. He is currently a Lecturer with the School of Information and Communication Engineering, BUPT. He serves as a member for the State Key Laboratory of Networking and Switching Technology, China. His research interests mainly include wireless testing theory, channel modeling, and the Internet of Things.

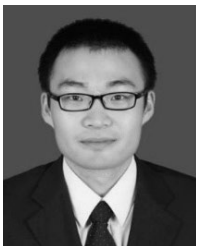

JIANQIAO CHEN received the M.S. degree from the Institute of Communications Engineering, Xidian University, China, in 2014. He is currently pursuing the Ph.D. degree with the Department of Information and Communication Engineering, BUPT. His research interests are in the areas of channel modeling and wireless communications.

PING ZHANG (Fellow, IEEE) received the Ph.D. degree from the Beijing University of Posts and Telecommunications (BUPT), China, in 1990. He is currently a Professor with the School of Information and Communication Engineering, BUPT. His research interest includes mobile communications.